RAYA JOURNAL OF SCIENCE AND DEVELOPMENT

RJSD 1(2):2026

Design and Numerical Analysis of Single-Tank Thermal Energy Storage System with Thermocline for Solar Thermal Applications

Amaha Kidanu Atsbeha[1*], Tesfay Abraha Berhe[1], Gebrekiros Gebreyesus Gebremariam[2], Mulu Tesfay Gebru [1], Higuse Gidey Weldegebriel[1], Kibrom Gidey Teklemariam[1]

[1]Department of Mechanical Engineering, Raya University, Main Campus, Maichew, P.O. Box 92, Tigray, Ethiopia

[2]Department of Electrical and Computer Engineering, Raya University, Main Campus, Maichew, P.O. Box 92, Tigray, Ethiopia

Email: amahakidanu12@gmail.com, tesfayabreha21@gmail.com, kiros2004comp@gmail.com, hagazi7744@gmail.com, higusgidey4@gmail.com, Kibromgidey12@gmail.com

Article History:
Received: 2025-12-12
Accepted: 2026-06-02
Published: 2026-07-07
DOI: https://doi.org/10.82489/rjsd.2025.1.01.39

Suggested citation:

Design and Numerical Analysis of Single-Tank Thermal Energy Storage System with Thermocline for Solar Thermal Applications. (2026). Raya Journal of Science and Development, 1(2). https://doi.org/10.82489/rjsd.2026.1.2.61

Correspondence :
Amaha Kidanu Atsbeha
amahakidanu12@gmail.com

Copyright:
©2026 Raya University, This is an open access article distributed under the terms of the Creative Commons Attribution License, which permits unrestricted use, distribution, and reproduction in any medium, provided the original author and source are credited.

Abstract

This study presents the design and numerical evaluation of a single-tank thermocline thermal energy storage (TES) system for solar thermal applications aimed at improving energy access in rural Ethiopia through small to medium-scale concentrated solar power (CSP) integration. A two-dimensional model using Computational Fluid Dynamics (CFD) and the Finite Element Method (FEM) simulated unsteady, incompressible laminar flow and heat transfer in a vertical cylindrical tank modelled as an isotropic porous medium. The system used water as the heat transfer fluid and operated between 55°C and 98°C, with a height-to-diameter ratio of 1.2. The computational mesh included 3,938 domain elements and 192 boundary elements, with a maximum element size of 0.01 m. During charging, hot water introduced at the top formed a thermocline that moved downward, reaching a thickness of 0.263 m after 7,200 seconds. The flow remained laminar, with a peak velocity of 0.02 m/s and a Reynolds number of about 1,078, while a pressure gradient of 2.49 kPa developed from top to bottom. The performance index was approximately 0.95, indicating strong stratification and minimal mixing. During discharging, reverse flow from the bottom reached a velocity of 0.002 m/s with a Reynolds number near 769, and the thermocline rose to 0.25 m by 7,200 seconds, maintaining separation of hot and cold zones. Enthalpy increased from 2.25 J/m³ to 2.55 J/m³ during charging and decreased from 4.0 J/m³ to 3.75 J/m³ during discharging, reflecting efficient energy storage and release. Overall, the results confirm stable thermal stratification, high energy efficiency, and the suitability of the proposed water-based thermocline TES for cost-effective, off-grid solar thermal energy applications.

Keywords: *Concentrated solar power, computational fluid dynamics, thermocline, thermal energy storage*

List of acronyms and their full description.

Acronyms	Full Name	Acronyms	Full Name
HTF	Heat Transfer Fluid	V	Velocity
TES	Thermal Energy Storage	V	Volume
CSP	Concentrated Solar Power	P	Pressure
DEM	Discrete Element Method	F	Body Force
CFD	Computational Fluid Dynamics	Re	Reynolds Number
CHP	Combined Heat and Power	G	Gravitational Acceleration Vector
CHT	Computational Heat Transfer	β	Thermal Expansion Coefficient
FEM	Finite Element Method	τ	Stress Tensor
FDM	Finite Difference Method	μ	Dynamic Viscosity
PV	Photovoltaic	m	Mass Flow Rate
H	Height	k	Thermal Conductivity

1. Introduction

The rising demand for clean energy has made solar thermal systems vital in reducing reliance on fossil fuels. However, the intermittent nature of solar radiation limits their reliability (Dincer & Rosen, 2011). Among TES methods, single-tank thermocline systems are preferred for their simplicity, lower cost, and reduced infrastructure needs. These systems use thermal stratification to separate hot and cold fluids within a single tank (S. Flueckiger et al., 2011). Filler materials like quartzite or silica rocks are added to improve heat capacity and maintain stratification by reducing fluid mixing (Zhang et al., 2016). Single-tank thermocline thermal energy storage systems provide a cost- and space-efficient alternative to traditional two-tank setups by utilizing natural fluid stratification, with water-based designs offering greater economic feasibility for low- to medium-temperature applications (Fernández et al., 2021; Lou et al., 2020, 2021; Qin et al., 2012). However, challenges such as thermocline degradation, limited understanding of key operational parameters, and oversimplified one-dimensional modelling motivate this study, which develops a detailed two-dimensional model to more accurately analyse flow, heat transfer, and stratification, thereby improving efficiency and addressing critical research gaps.

Many rural communities in Ethiopia lack access to reliable grid electricity and depend on costly diesel generators, biomass, and kerosene, which limit basic needs such as lighting, cooking, and refrigeration while contributing to deforestation and health risks from smoke exposure. Small- to medium-scale concentrated solar power (CSP) (Atsbeha et al., 2026; Kahsay et al., 2025) systems present a clean and sustainable alternative, but their reliability depends on integrating thermal energy storage (TES) to overcome solar intermittency. Although water-based single-tank thermocline TES offers a cost-effective and locally adaptable solution, such systems remain underdeveloped in Ethiopia and performance data is limited. This project therefore aims to design and simulate a single-tank thermocline TES system for solar thermal applications, focusing on optimizing heat transfer and storage efficiency to support CSP deployment in rural communities. By reducing material costs, minimizing energy losses, and improving power reliability, the proposed system can enhance the feasibility of off-grid solar solutions, guide future prototype development, and support sustainable energy policies to bridge the energy gap in Ethiopia's underserved regions.

A thermocline thermal energy storage (TES) tank stores hot fluid at the top and cold fluid at the bottom, separated by a sharp temperature gradient called the thermocline (Zhu et al., 2022). This stratification allows a single tank to act as both hot and cold reservoirs, reducing cost and space compared to two-tank systems (Inlet, 2023). Ideally, the thermocline would be infinitesimally thin, maximizing efficiency, but in practice, mixing causes it to thicken over time (Angelini et al., 2014). Solar energy (Atsbeha et al., 2024, 2025), mainly harnessed through photovoltaic (PV) and solar thermal systems, benefits from TES integration, which enables energy use during cloudy periods or at night through repeated charging, storing, and discharging cycles (Dincer, 2002). Among TES methods, sensible heat storage is the simplest, relying on temperature changes without phase transitions. Water, due to its high specific heat capacity, low cost, and effectiveness below 100 °C (Atsbeha & Gebremariam, 2026), is a particularly suitable medium, and the stored heat is calculated as:

$$Q = \int_{T_i}^{T_f} mC_P dT \quad = \quad mC_P(T_F - T_i) \tag{1}$$

Where $Q =$ Amount of thermal energy $\frac{\text{stored}}{\text{released}}$ in the form of sensible heat (KJ)

$m =$ The mass of material used to store thermal energy (kg)

$C_P =$ the specific heat of the material to store thermal energy $\left(^{KJ}/_{Kg°C}\right)$

$T_F, T_i =$ final and initial temperature (°C), respectively

When mass is expressed in terms of density and volume, the equation takes the following form:

$$Q = \rho * C_P * V * (T_F - T_i) \tag{2}$$

where, ρ: density of the storage material $[kg/m^3]$ and

V: volume occupied by the storage material $[m^3]$

This equation is very important to bear in mind when choosing the storage materials, the important thermal properties are the volumetric heat capacity ($\rho * C_P$), which dictates the energy storage density capability, and the heat diffusivity ($\frac{\lambda}{\rho * C_P}$), which reflects the rate of the heat released and absorbed. Latent heat storage uses phase change materials like paraffins and salt hydrates to store energy during melting and solidifying, offering higher energy density and stable temperatures compared to sensible heat storage (*A1234.Pdf*, n.d.). However, it faces challenges like low thermal conductivity, subcooling, and higher material costs. The stored thermal energy of PCM at different heating stages can be calculated as follows:

$$Q = \int_{T_1}^{T_2} m.C_{P,S}\,.\,dT \tag{3}$$

$$Q = \int_{T_1}^{T_m} m.C_{P,S}\,.\,dT + m.\Delta H_m \tag{4}$$

$$Q = \int_{T_1}^{T_m} m.C_{P,S}\,.\,dT + m.\Delta H_m + \int_{T_m}^{T_2} m.C_{P,l}\,.\,dT \tag{5}$$

Where, T_m: temperature of the phase change, ΔH_m: enthalpy of the phase change, $C_{P,S}$: solid phase PCM heat capacity, $C_{P,l}$: liquid phase PCM heat capacity

Single-tank thermocline thermal energy storage (TES) systems provide a cost-effective alternative to conventional two-tank designs, reducing capital costs by nearly one-third, with natural rock fillers lowering overall CSP plant costs by up to 35% (Boubou et al., 2021). Research emphasizes maintaining thermal stratification and minimizing mixing through optimized flow design, porosity adjustment, and filler selection, with studies showing efficiency gains of 30–70% depending on parameters such as HTF velocity, filler sphericity, and tank sectioning (Al, 2012; Jadhav et al., 2020; Şentürk Lüle & Asaditaheri, 2022; Types, 2024; Z. Yang & Garimella, 2010). Low-cost fillers like quartzite and alumina improve stratification and storage duration (Bayón & Rojas, 2014; Cascetta et al., 2021; He, Wang, et al., 2019; Li et al., 2018; Mira-Hernández et al., 2015). while phase change materials (PCMs) offer higher energy density but face challenges in control and efficiency (Bonanos & Votyakov, 2021; Guo et al., 2021). Despite extensive numerical work, experimental studies remain limited, with most simulations employing porous-medium and CFD-based models to capture transient heat transfer and flow dynamics (Bayón et al., 2014; S. M. Flueckiger & Garimella, 2012; Ismail & Stuginsky, 1999). Thermocline TES systems fall within broader TES categories sensible, latent, and thermochemical storage (Chang et al., 2020; Review, 2024). Recent CFD studies highlight the importance of axial porosity, outlet temperature distribution, charging time, and pressure drop in performance optimization (Alptekin & Ezan, 2020; Elfeky et al., 2022; He, Qian, et al., 2019; Hoffmann et al., 2016; Hu et al., 2020; Junli et al., 2023; X. Yang & Cai, 2019). In CSP plants, thermocline tanks operate as thermal batteries, storing excess solar heat in hot and cold layers for later discharge to drive steam turbines. Literature consistently shows that with proper flow control, intermediate height-to-diameter ratios (H/D ≈ 1–2), and structural provisions for thermal expansion, single-tank TES can match the thermal performance of two-tank systems while significantly reducing cost, making them highly suitable for future CSP deployment.

The objective of this study is to design and numerically evaluate a water-based single-tank thermocline thermal energy storage (TES) system for solar thermal applications, focusing on optimizing thermal stratification, minimizing mixing, and improving heat transfer efficiency. The significance of this research lies in providing a cost-effective, locally adaptable solution for off-grid concentrated solar power (CSP) deployment, particularly in rural Ethiopian communities (Kahsay et al., 2025), by reducing material costs, enhancing energy reliability, and supporting sustainable energy policies. The findings aim to guide future prototype development, inform CSP system design, and contribute to bridging the energy access gap in underserved regions.

2. METHODOLOGY

2.1 Tank Design and Geometry

The thermocline tank is a vertical cylindrical vessel designed to hold the water volume corresponding to both the hot and cold fluid inventory. Based on the assumed 625 $\frac{m^3}{h}$ flow, and a target of at least ~4 hours of storage, a volume on the order of 1250 m^3 is needed. We take tank height of 26.3688 m and a diameter of 21.974 m. This geometry yields an aspect ratio of H/D ≈ 1.2, within the range found effective in literature for good stratification (Zhu et al., 2022). The storage tank is designed for a discharge period of 4 hours and an operating temperature between 55ºC and 98ºC (Zhu et al., 2022). A working fluid of liquid water is used to store the required energy. Those values are tried to scale down by 100 and the scaled values are summarized in Table 1.

Table 1

Summary of scaled-down values.

Parameter	Original (m)	Scaled Values (m)	Change
Height	26.3688	0.263688	÷100
Diameter	21.974	0.21974	÷100
Volume	1250 m^3	0.00125 m^3	÷1M
Flow rate	625 m^3/h	0.000625 m^3/h	÷1M
Inlet velocity	0.00045779 m/s	0.00045779 m/s	Same
Energy storage capacity	Q	Q ÷ 1000000	÷ 1M
Charging/discharging time	t	t ÷ 10000	÷ 10k

The materials used to model the thermocline packed bed thermal energy storage with sensible filler are: Heat Transfer Fluid (HTF)**:** Used to transport heat from the heat source (solar collector) to the storage tank during charging and to transfer heat from the storage tank to the load (boiler) during discharging. Sensible liquid water (sensible storage), Tank wall material (steel wall and insulation material), Modelling tools (Ansys fluent, COMSOL, and Excel)

The required parameters specifications/ assumptions for the modeling of the system are: HTF operating temperatures: the selected heat transfer fluid temperatures are, 371.15 k cold temperature and 328.15 k hot temperature. Tank Material: Steel is used for constructing the tank wall, while wood ash serves as the insulating material for the tank. System Layout**:** The system features a thermocline tank filled with liquid water, storing both hot and cold energy in a single tank hot fluid is located at the top, while cold fluid remains at the bottom, as shown in Figure *1*. The cylinder is installed vertically with a charging inlet at the top and a discharging inlet at the bottom. Figure 1 illustrates the typical configuration of the thermocline TES tank and the computational domain. The system comprises a vertical cylindrical tank that utilizes solid particles as the heat storage medium, forming a packed-bed thermal storage area.

Additionally, the inlet and outlet ports, located at the top and bottom of the tank, enable the flow of HTF in and out of the tank.

Figure 1

The computational domain of the charging and discharging process.

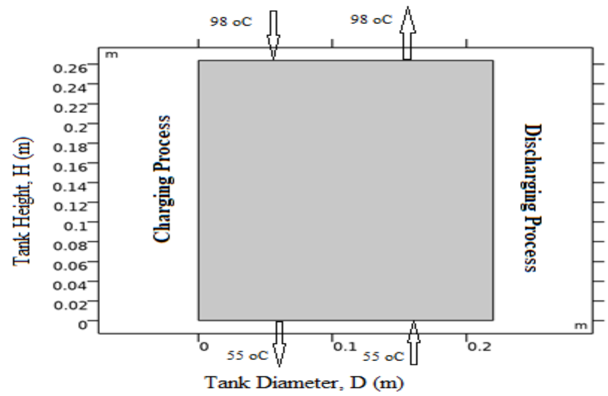

For choosing tank height and diameter dimensions, we considered the relation bellow diameter/height: The Hight and diameter of the tank can be selected based on the Ansys fluent simulation of the best height to diameter ratio.

$$V_{tank} = \pi * \left(\frac{D}{2}\right)^2 * H \tag{6}$$

Table ***1*** the flow rate is proportionally scaled down by 100 and the inlet velocity is almost similar V_1 = 0.00045779 m/s So, to determine the small inlet tank velocity or the asymmetric velocity apply the continuity equation as 0.001831m/s.

$$D_{tank} = 21.974 \text{ meter and } H = 26.3688 \text{ meter}$$

Q = A× V = 625 $\frac{m^3}{h}$ = $\pi * \left(\frac{D1}{2}\right)^2 \times V_1$ but D_1 = 21.974 m and D_2 = 0.21974 m which is small diameter and from Table 1.

2.2 Mathematical Model

The continuity equation in a cylindrical coordinate system is expressed as follows:

$$\nabla . u = 0 \tag{7}$$

Where ∇ = delta operator" or "gradient operator, u = u_r, u_θ, uz

Equation (7) applies to incompressible fluids, where ρ (r, z, t) = c, with t representing time, and z and r denoting the axial and radial directions, respectively.

In cylindrical coordinates (r, θ, z), the divergence of the velocity field u = (u_r, u_θ, u_z) is given by:

$$\nabla . u = \frac{1}{r}\frac{\partial(rur}{\partial r} + \frac{1}{r}\frac{\partial U\theta}{\partial \theta} + \frac{\partial Uz}{\partial z} \tag{8}$$

For an incompressible fluid, the density ρ is constant, which implies that the divergence of the velocity field must be zero:

$$\nabla . u = 0 \tag{9}$$

By substituting the expression for the divergence in cylindrical coordinates, we obtain:

$$\frac{1}{r}\frac{\partial(rur}{\partial r} + \frac{1}{r}\frac{\partial U\theta}{\partial \theta} + \frac{\partial Uz}{\partial z} = 0 \tag{10}$$

This equation indicates that the overall divergence of the velocity field, including its radial, angular, and axial components, must be zero for the fluid to remain incompressible. This condition corresponds to the continuity equation in cylindrical coordinates for an incompressible fluid.

The form of the momentum equation in a cylindrical coordinate system is as follows:

$$\rho\frac{\delta u}{\delta t} + \rho(u.\nabla)u = -\nabla p + \nabla . T + f \tag{11}$$

where: ρ is the fluid density, u is the velocity vector, p is the static pressure, τ is the stress tensor, f represents body forces (e.g., gravity).

The stress tensor τ for a Newtonian fluid is given by:

$$\tau = \mu\, [(\nabla . u + (\nabla . u)^T\,] \tag{12}$$

where μ is the dynamic viscosity.

Body Force: The body force term f can include various forces such as gravitational force. In this case, it is given by:

$$F = -\rho\beta + (T - T_{ref}).\, g \tag{13}$$

where: β is the thermal expansion coefficient, T is the temperature, T_{ref} is the reference temperature, g is the gravitational acceleration vector. In cylindrical coordinates (r, θ, z), the components of the momentum equation are as follows:

$$\rho\left(\frac{\delta U_r}{\delta t} + u_r\frac{\delta U_r}{\delta r} + \frac{U_\theta}{r}\frac{\delta U_r}{\delta \theta} - \frac{U2\theta}{r} + u_z\frac{\delta U_r}{\delta z}\right) = -\frac{\delta p}{\delta r} + \mu\left(\nabla^2 u_r - \frac{U_r}{r2} - \frac{2}{r2}\frac{\delta U_\theta}{\delta \theta}\right) + F_r \quad (14)$$

$$\rho\left(\frac{\delta U_\theta}{\delta t} + u_r\frac{\delta U_\theta}{\delta r} + \frac{U_\theta}{r}\frac{\delta U_\theta}{\delta \theta} + \frac{U_r.U_\theta}{r} + u_z\frac{\delta U_z}{\delta z}\right) = -\frac{1}{r}\frac{\delta p}{\delta \theta} + \mu\left(\nabla^2 u_\theta + \frac{2}{r2}\frac{\delta U_r}{\delta \theta} - \frac{U_\theta}{r2}\right) + F_\theta \quad (15)$$

$$\rho\left(\frac{\delta U_z}{\delta t} + u_r\frac{\delta U_z}{\delta r} + \frac{U_\theta}{r}\frac{\delta U_z}{\delta \theta} + u_z\frac{\delta U_z}{\delta z}\right) = -\frac{\delta p}{\delta z} + \mu\nabla^2 u_z + F_r \quad (16)$$

Combining these components, we get the momentum equation in cylindrical coordinates:

$$\rho\frac{\delta u}{\delta t} + \rho\,(u.\nabla)u = -\nabla p + \nabla.\,T - \rho\beta(T - T_{ref})g \quad (17)$$

The temperature distribution is determined using the diffusion/convection equation, as shown below:

$$\rho\, c_p\frac{\delta T}{\delta t} + \rho\, c_p\, u.\,\nabla T = -\nabla.\,(\lambda\nabla T \quad (18)$$

where Cp represents the specific heat capacity at constant pressure and λ denotes the thermal conductivity.

The standard turbulence model is used as follows:

$$\frac{\delta}{\delta t}(\rho k) + \nabla.\,(\rho u k) = \left[\left(\mu + \frac{\mu t}{\sigma k}\right)\nabla k\right] + G_k + G_b + \rho\varepsilon \quad (19)$$

$$\frac{\delta}{\delta t}(\rho\varepsilon) + \nabla.\,(\rho u k) = \nabla.\,(\Gamma_\varepsilon\nabla_\varepsilon) + \rho\frac{\varepsilon}{k}(c_1 G - c_2\varepsilon) \quad (20)$$

where Gk is the turbulent kinetic energy generated by the velocity gradient, Gb is the turbulent kinetic energy generated by buoyancy, k $ ε are fluid turbulent kinetic energy and turbulent dissipation rate, respectively.

2.3 Computational Method and Fluid Dynamics

Mechanical and thermal issues in complex systems can be addressed through experimental, analytical, or numerical approaches, with numerical methods often preferred for intricate problems. Computational Fluid Dynamics (CFD) and Computational Heat Transfer (CHT) are key numerical tools that solve the Navier–Stokes and energy equations, respectively, using techniques such as finite difference, finite volume, and finite element methods. Advances in computing power and software have greatly enhanced their accuracy and efficiency, making them essential for analyzing fluid flow, heat transfer, and complex interactions across engineering applications. In this study, the Finite Element Method is employed to develop a two-dimensional model of a thermocline

thermal energy storage (TES) tank treated as an isotropic porous medium with solid spherical particles. By discretizing the domain into finite elements and using Backward Differentiation Formula (BDF) for time integration, FEM effectively captures flow patterns and heat transfer, while exploiting symmetry to simplify computations and accurately predict the tank's thermal behavior. Results will be validated against literature and visualized through 2D isothermal contours

and streamlines, illustrating temperature, time, and spatial relationships and its numerical process is summarized in Figure 2.

Figure 2

Flow chart of the numerical process.

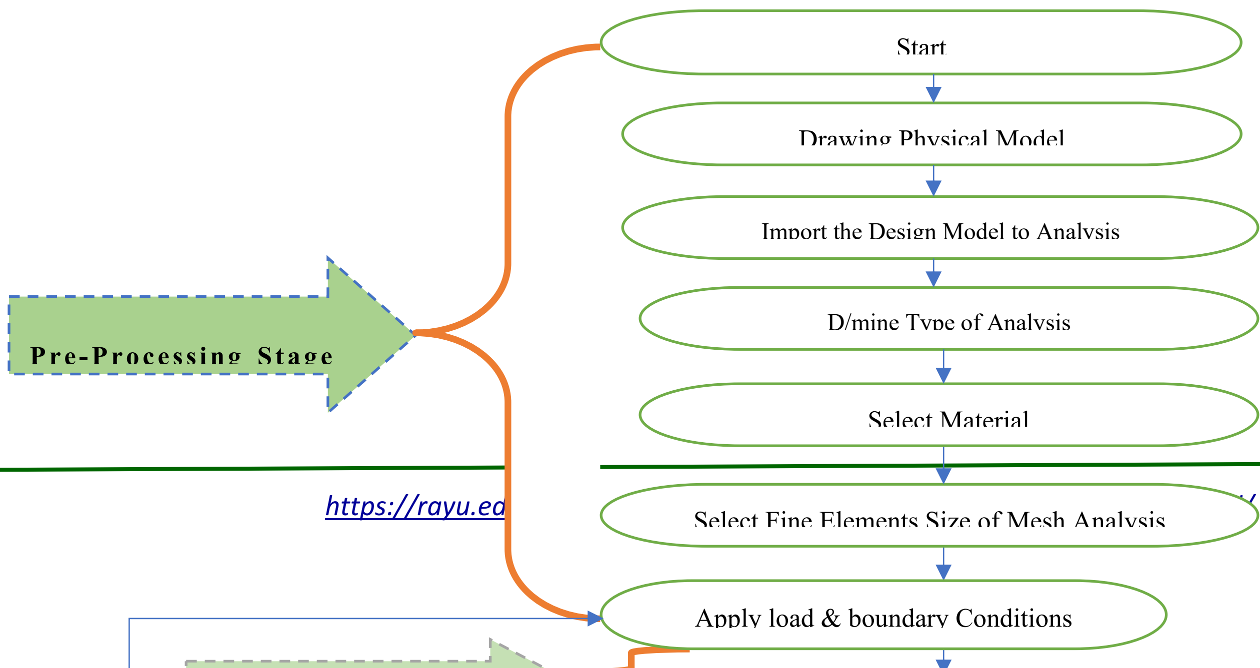

2.4 Boundary Conditions and Solver Settings

The straightforward design of the single storage tank allows for the use of a structured quadrilateral element grid and an axisymmetric plane model for simulation. Calculations are carried out using Fluent's two-dimensional, double-precision solver, which utilizes a coupled, implicit, and axisymmetric approach to ensure both accuracy and efficiency. The physical model incorporates unsteady heat transfer and a turbulence model.

$$Re = \frac{\rho u D}{\mu} \qquad (20)$$

(Re = $\frac{\rho u D}{\mu} = \frac{985\,\frac{kg}{m3} \times 1.831 \times 10^{-3}\frac{m}{s} \times 0.21974\ m}{3.667 \times 10^{-4} Pa.s}$ = 1078, indicates laminar flow (typical for inlet pipes or high velocities). Turbulence generally occurs for Re>4000 during charging process and Re = $\frac{\rho u D}{\mu} = \frac{962.01\,\frac{kg}{m3} \times 1.831 \times 10^{-3}\frac{m}{s} \times 0.21974\ m}{5.04 \times 10^{-4} Pa.s}$ = 769, The very low Reynolds number indicates that the flow remains fully laminar throughout the discharging process. In the simulation, the inlet and outlet are defined as a velocity inlet and outflow, respectively. To simplify the model, several assumptions are made: the tank is rigid, cylindrical, and adiabatic; the flow is incompressible; the porous filler is homogeneous with constant porosity; only the charging process is considered; radiation and phase change effects are neglected; and water is used as the working fluid with constant thermal properties.

2.5 Physical Parameters of Working Fluid

The working fluid is water, operating at standard pressure with temperatures ranging from 328.15 K to 371.15 K. Using the physical property data for water, fitting correlations have been developed to calculate the fluid's density, dynamic viscosity, and thermal conductivity within this temperature range. The overall properties of water during the charging and discharging processes are summarized in

$$k = -46.99 + 24.106 \times (1 - e^{-\frac{T}{48.09069}}) + 23.58177 \times (1 - e^{-\frac{T}{48.10424}}) \qquad (23)$$

Table ***2***.

$$\rho = 866.19608 + 1.22008T - 0.00261T^2 \qquad (21)$$

$$\mu = \frac{1.779 \times 10^{-5}}{8.276269 - 0.086986T + 0.00221T^2} \qquad (22)$$

Table 2

Properties of water during charging (55 °C) & discharging (98 °C) process.

No.	Parameters	Charging Process (T = 55 °C)	Discharging Process (T = 98 °C)
1	Density (ρ)	985 kg/m^3	962.01 kg/m^3
2	Dynamic viscosity (μ)	0.3667×10^{-3} pa. s = 3.667×10^{-4} kg/m. s	0.5036×10^{-3}pa. s = 5.036×10^{-4} kg/m. s
3	Specific heat (Cp)	4.18 kj/kg. °C	4.18 kj/kg. °C
4	Thermal conductivity (k)	0.630 W/(m·K)	0.662 W/(m·K)

2.6 Mesh Generation

Mesh generation divides a continuous domain into finite elements to enable numerical analysis. In this study, a structured quadrilateral mesh was used for the rectangular thermal energy storage tank, providing numerical stability, accurate gradient calculations, and reduced discretization errors compared to triangular meshes. Tetrahedral and hexahedral elements fill the tank's fluid volume to support solutions of governing equations such as the Navier–Stokes equations. Boundary conditions, including no-slip walls and pressure outlets, are applied appropriately, with a finer mesh near walls to resolve high-gradient regions. The final mesh consists of 3,938 domain elements and 192 boundary elements, achieving a balance between computational efficiency and simulation accuracy. Key mesh parameters are summarized in

Table *3*. Taking mesh element size = 0.01 and velocity = 0.001831 m/s so the time step size is calculated as:

$$\text{Time step size} = \frac{\text{mesh Element size (m)}}{\text{inlet velocity } (\frac{\text{m}}{\text{s}})} \tag{24}$$

Table 3

Some of the main mesh element parameters.

No.	Mesh Parameters Values	Values
1	Maximum element size	0.001 m
2	Minimum element size	2.2 × 10^{-4} m
3	Maximum element growth rate	1.15
4	Resolution of Curvature	0.3
5	Resolution of narrow regions	1
6	Predefined size	User Defined

Figure 3

2D Mesh of Tank Geometry and Internal Fluid Domain

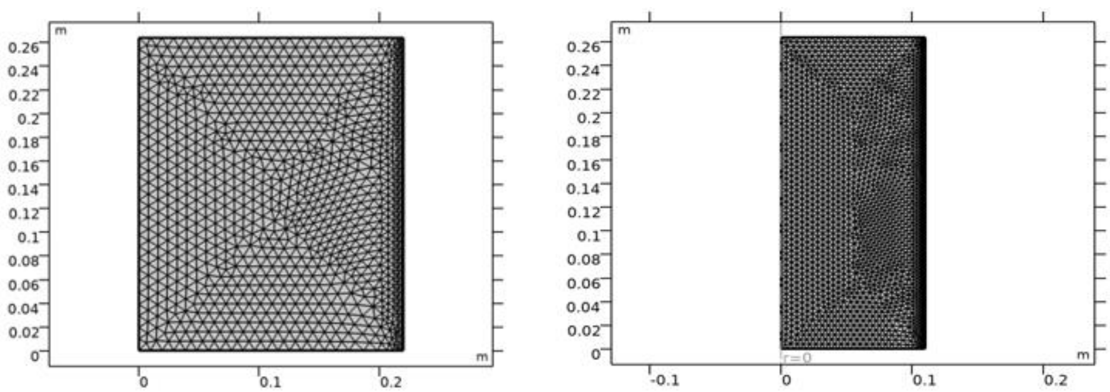

The two-dimensional mesh layout within the storage tank is shown in Figure 3. Choosing an appropriate mesh for a specific model generally involves selecting suitable element types and sizes. In this study, the Quadrilateral Meshing technique is applied. Due to the axisymmetric nature of the model, only the right half of the tank is meshed. The maximum element growth rate controls how much the element size can increase from finer to coarser regions and must be equal to or greater than one. Here, it is set to 1.15, allowing the element size to grow by up to 25% between adjacent elements. The curvature factor represents the ratio of the boundary element size to the radius of curvature, with the product of these two values determining the maximum allowable element size along curved boundaries. A lower curvature factor results in a finer mesh in those regions.

2.7 Mesh Independence Test

Figure 4

Temperature profiles along the tank axis for three different Mesh Sizes and grid numbers

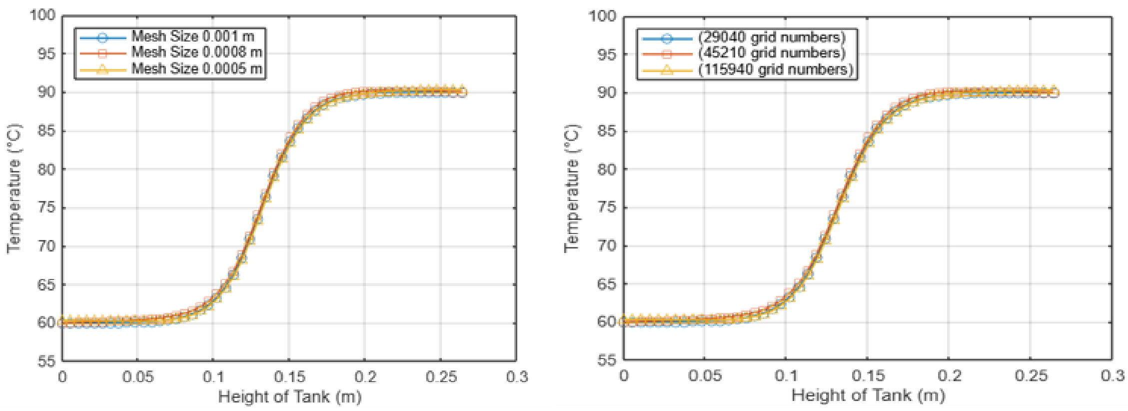

.

As shown in Figure **4**, the mesh size and grid density significantly influence the temperature distribution within the TES tank. Across all mesh sizes (0.001 m, 0.0008 m, 0.0005 m) and grid counts (29,040, 45,210, 115,940), temperature rises from approximately 60 °C at the bottom to around 90 °C at the top, reflecting effective thermal stratification. Smaller mesh sizes and higher grid densities improve the resolution of transient temperature gradients but have minimal impact on the final steady-state distribution. Similarly, temperature profiles along the tank wall for varying mesh dimensions show negligible differences, validating that a maximum mesh size of 0.001 m provides sufficient accuracy. These results confirm the robustness of the model and its reliability for simulating thermal behavior in the charging phase of the tank.

3. Results and Discussion

3.1 Thermal Performance Results (CFD)

CFD simulations of the charging process show the gradual formation and downward movement of the thermocline layer within the tank. Initially at 55 °C, the tank develops a hot layer at the top as 98 °C water is injected, with a sharp interface indicating effective stratification. Over time, the thermocline moves downward as the hot region expands, limiting the volume of high-temperature water available for storage and slightly reducing TES performance. A thicker thermocline further lowers efficiency, making thermocline thickness a critical parameter for evaluating system performance using the TES performance index.

$$k = 1 - \frac{\delta}{H}$$

In this study, the thermocline thickness δ and the tank height H are key indicators of thermal stratification in the TES system, with a higher performance evaluation index reflecting greater efficiency. Numerical simulations were performed using liquid water as the heat transfer fluid to examine how time and flow velocity affect temperature distribution. Initially, the thermocline is very thin, representing the mixing zone between incoming hot water and initially cold fluid, and it grows to approximately 0.263 m during charging. Despite this expansion, the thermocline remains much smaller than the total tank height, ensuring that most of the tank volume is effectively hot or cold. The performance evaluation index reached about 0.95, indicating only ~5% energy loss due to mixing. This high stratification efficiency results from low inlet velocity and density-driven stabilization, aligning with previous findings of ~95–96% efficiency for water-based thermocline TES tanks (Bouhlel et al., 2023).

3.2 During the charging process

3.2.1 Pressure and Velocity Profile for Charging Process

In this analysis, diagrams illustrating velocity, pressure distribution, and streamlines for single-phase liquid water during the charging phase are presented. Liquid water serves as the heat transfer fluid (HTF) within the thermal energy storage (TES) tank. The observed flow characteristics closely resemble those obtained using other HTF configurations, indicating consistency in fluid behavior. These visual representations effectively convey the internal dynamics of fluid motion, pressure variation, and streamline development within the storage system. The velocity distribution, in particular, is a critical indicator for interpreting and analyzing the flow behavior. Simulation results provide insights into velocity magnitudes for each material up to a 120-minute duration. Since the flow characteristics remain largely unchanged throughout the charging cycle, the velocity field, pressure distribution, and streamline plot are all depicted at the 120-minute mark (equivalent to 7200 seconds).

Figure 5

Velocity magnitude distribution across the entire surface of the TES tank during the charging cycle and Enlarged view of the velocity field near the tank wall, highlighting detailed flow behavior during charging.

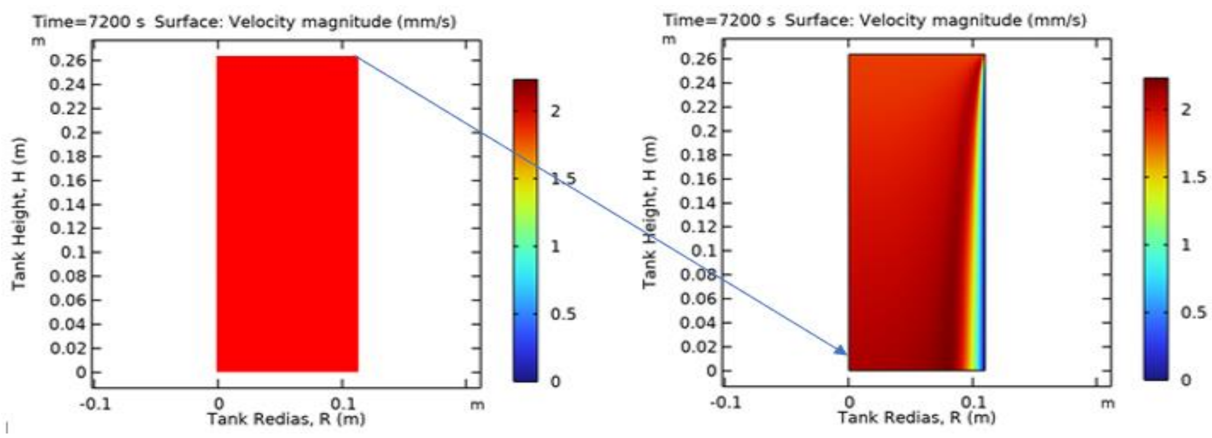

Throughout the charging and discharging phases of a thermal energy storage (TES) system utilizing liquid water as the heat transfer medium, pressure contour plots may reveal regions of negative gauge pressure within the tank. These low-pressure zones typically arise when internal tank pressure drops below atmospheric levels, which can result from phenomena such as thermal contraction during the cooling phase, rapid fluid outflow during discharge, or irregular thermal expansion during the charging process. In systems that are sealed or insufficiently vented, such conditions may lead to the formation of partial vacuums, particularly around inlet and outlet ports or near the tank's upper section. While these negative pressure areas are commonly observed in simulation environments, they can also occur in actual systems lacking proper pressure regulation. If unaddressed, such pressure imbalances can contribute to structural stress, initiate cavitation, or allow air to enter the system.

As illustrated in Figure 5, the velocity magnitude within the TES tank varies during the charging phase. In this stage, the heated fluid descends from the top of the tank toward the bottom. Figure 5 displays the velocity field across the entire tank, while a detailed view focused on the region adjacent to the tank wall. This localized view reveals that variations in velocity magnitude are primarily confined to a narrow zone along the tank's boundary. To enhance visual interpretation, a color-coded scale is used to represent the velocity values red indicates higher velocities, while blue denotes lower ones. The peak velocity observed within the tank reaches up to 0.02 meters per second.

Figure 6

Pressure contour inside of the TES tank for charging cycle.

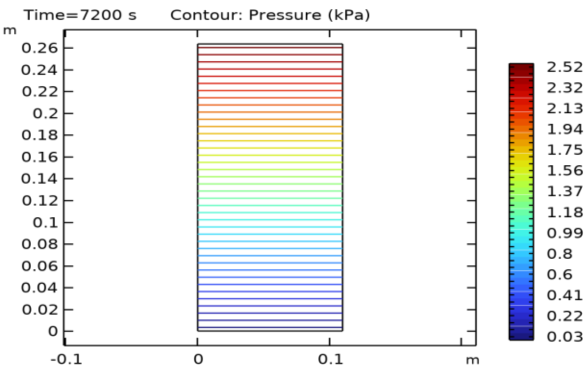

Figure 7

Streamline distribution inside the TES tank during the charging cycle

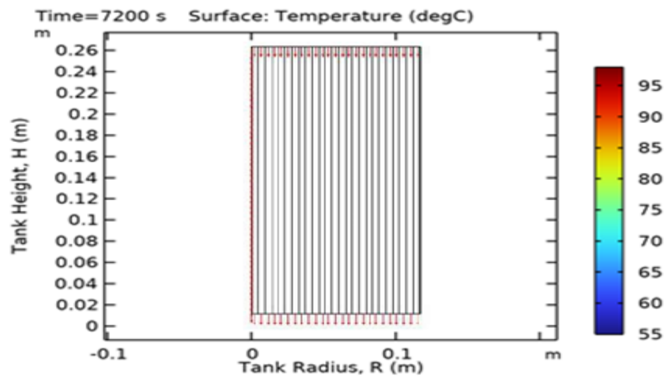

As shown in Figure 6, the gauge pressure contour illustrates the pressure distribution inside the TES tank. A pressure contour represents lines of equal pressure, also known as isobars. As shown in the figure, there is a slight pressure gradient from the top to the bottom of the tank. Specifically, the gauge pressure near the top surface is approximately 2.52 kPa, while at the bottom it drops to around 0.03 kPa. This creates a pressure difference of approximately 2.49 Pa between the two points. Although measurable, this variation is relatively small compared to atmospheric pressure, indicating a modest internal pressure distribution during the charging phase. The above Figure 7 illustrates the streamline distribution within the TES tank, with arrow lines indicating the direction of fluid flow. The streamline pattern reveals that the flow remains laminar throughout the tank, with no evidence of turbulence or flow separation.

The directional arrows clearly depict a downward movement of the fluid, consistent with the charging process, where hot fluid enters from the top and moves downward through the packed bed. The smooth and orderly nature of the streamlines confirms stable and controlled flow behavior during this phase of operation, which is essential for maintaining thermal stratification and efficient energy storage.

3.2.2 Temperature Profile During Charging Process

The temperature profile serves as a vital tool in heat transfer analysis, representing the distribution of temperature across each segment of the 2D geometry. Since the study involves transient heat transfer, the temperature of every individual mesh element can be tracked at specific time intervals. In this section, the temperature distribution along the vertical height of the storage bed is presented for various moments during the charging process. Additionally, surface temperature variations of the TES tank are displayed for different heat transfer fluids. To enhance clarity, line graphs of the surface temperature profiles are included, providing insight into how the temperature gradients develop over time. Due to the axial symmetry of the TES tank, the simulation is conducted on one-half of the tank geometry, allowing the analysis to focus on a representative portion. The resulting 2D surface temperature distribution provides a realistic depiction of thermal behavior within the tank, illustrated through a color-coded scheme. The simulation spans a total duration of 120 minutes (7,200 seconds), enabling clear visualization of the evolving temperature profile over time. In this analysis, liquid water is used as the heat transfer fluid, with its temperature ranging from 55 °C to 98 °C. Temperature profiles are presented at specific time intervals: 0 seconds, 1,800 seconds, 3,600 seconds, 5,400 seconds, and 7,200 seconds. The initial three sub-sections of this section focus on a single-stage thermal energy storage configuration, where the tank is entirely filled with a uniform phase.

Figure 8

Presents: (A–E) two-dimensional representations of the temperature profile within the TES tank at 0, 1800, 3600, 5400, and 7200 seconds, respectively; and (a–e) line graphs showing the variation of temperature with tank height at the same time interval

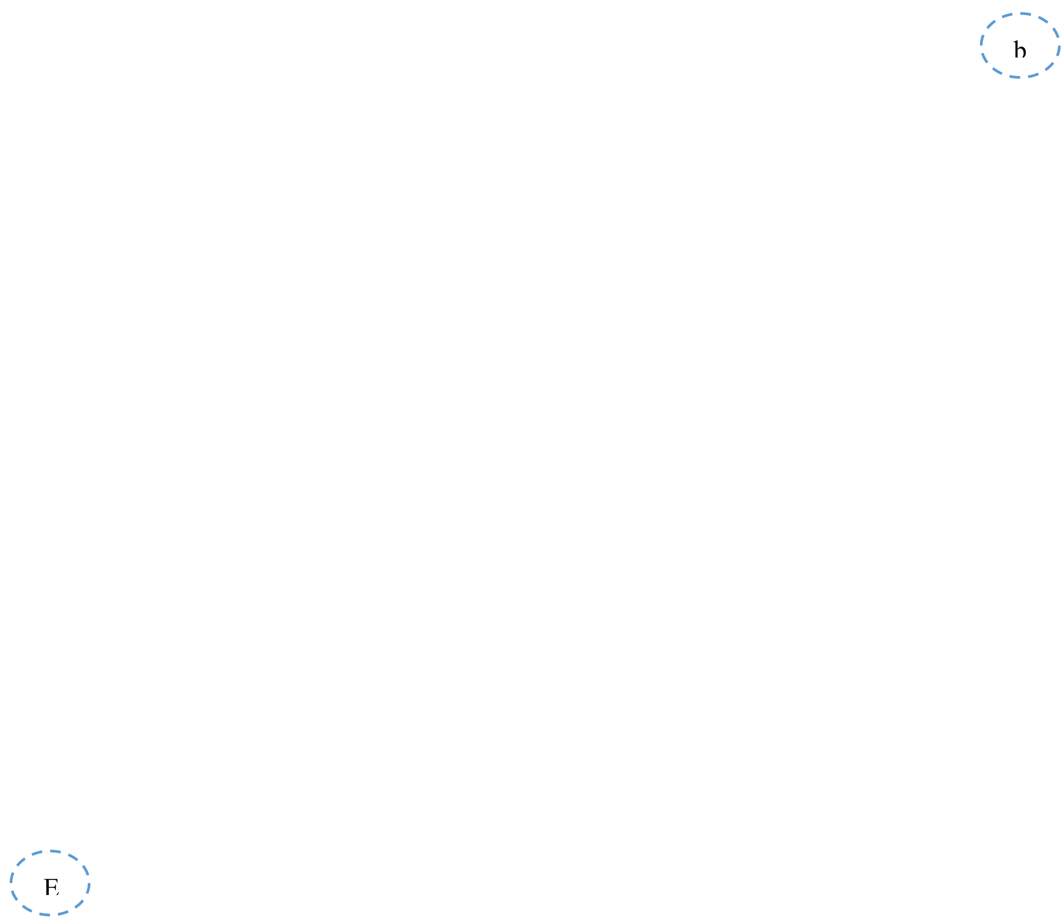

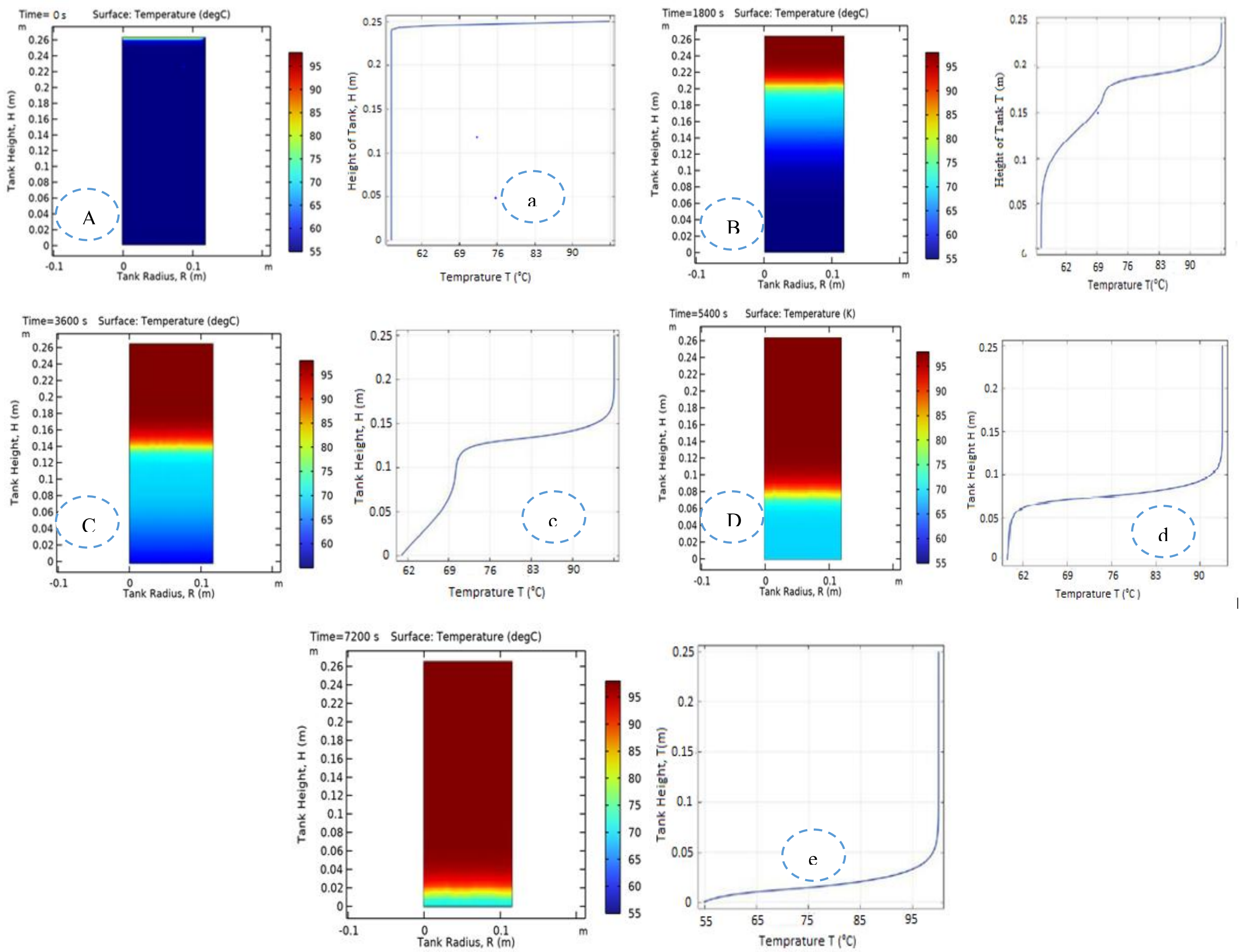

The above Figure 8 displays the thermal behavior within the 2D domain of the TES tank during the charging process. Sub Figure 8 (A–E) illustrates the temperature distributions at various time steps, while Sub Figure 8 (a–e) presents the corresponding line plots for each time interval. In the color-coded diagrams, blue represents lower (colder) temperatures, and red indicates higher (hotter) temperatures. At the initial moment (0 seconds), the entire tank is at the baseline temperature of 55 °C, reflecting the initial condition. A slight temperature gradient can be observed near the top surface of the tank, which occurs as the incoming hot fluid begins to interact with the colder fluid already present.

By 1,800 seconds, a distinct thermocline zone emerges around 0.2 m from the bottom of the tank, where the temperature transitions rapidly this is clearly visible in Figure 8(a). The steep gradient in this region signifies the development of the thermocline, a narrow zone separating the hot and cold fluid layers. As the process continues, the thermocline moves downward, appearing near 0.14 m at 3,600 seconds, 0.08 m at 5,400 seconds, and 0.02 m at 7,200 seconds. The slope of the temperature curve reflects the sharpness or thickness of the thermocline layer, with a steeper gradient indicating a thinner thermocline zone. A thinner thermocline is considered more effective, as it minimizes heat diffusion into the colder regions below. However, over time, the thermocline gradually flattens due to ongoing heat transfer from the hot fluid to the cold. In all cases, the region above the thermocline maintains a temperature close to the inlet fluid, while the region below remains at the lower, initial temperature.

3.3 During the Discharging Process

3.3.1 Pressure and Velocity Profile for Discharging Process

Figure 9

(a) Velocity magnitude (mm/s) across the entire surface of the TES tank, and (b) a detailed view near the tank wall during the discharging cycle.

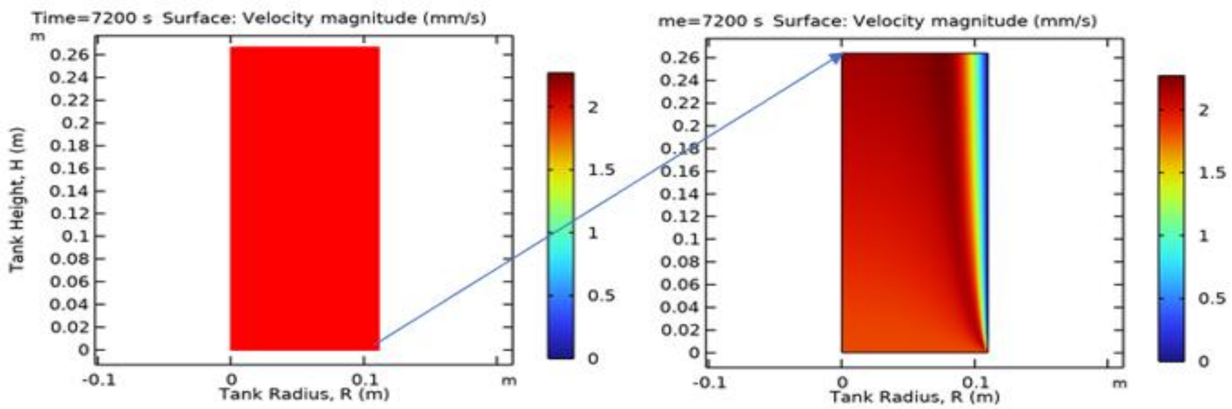

As shown in Figure 9 illustrates the velocity magnitude within the TES tank during the discharging cycle, which is the reverse of the charging process. In the discharging phase, hot fluid moves from the bottom to the top of the tank. Panel on the lest side shows the velocity distribution across the entire tank, while panel on the right focuses on a zoomed-in view near the tank wall. As observed in the charging cycle, velocity variations are seen near the tank boundary, though they are confined to a narrow region close to the wall. For clarity, a color scale is used to represent the velocity magnitudes, with the maximum velocity recorded in the tank being 2 mm/s.

Figure 10

Pressure contour within the TES tank during the discharging cycle.

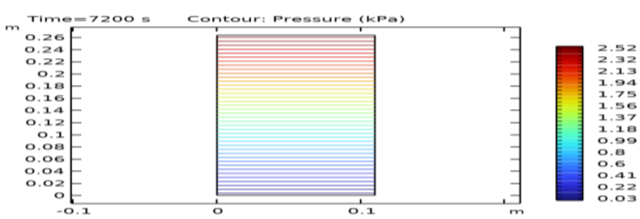

Figure 11

Streamlines within the TES tank during the discharging process.

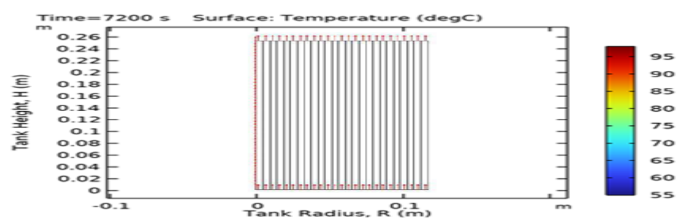

The above Figure 10 presents the gauge pressure contour inside the TES tank during the discharging cycle. In contrast to the charging cycle, the pressure is slightly higher near the bottom of the tank, where the fluid enters, and gradually decreases toward the top. Specifically, the pressure at the bottom is approximately 2.52 kPa, while at the top it is about 0.03 kPa, resulting in a pressure difference of roughly 2.49 kPa, which remains relatively low.

The streamlines within the TES tank, with the upward arrows indicating the flow direction as shown in Figure 11. This flow is opposite to that observed during the charging cycle.

3.4 Temperature Distribution for discharging Process

This section presents the temperature profile along the bed height at various time intervals during the discharging cycle. In this phase, the heat transfer fluid enters the TES tank from the bottom. Surface temperature profiles of the TES tank are shown for different heat transfer fluids, each corresponding to its respective phase. These are accompanied by line graphs to illustrate the development of temperature profiles over time. The data presented in this section specifically uses liquid water as the heat transfer fluid, with temperatures ranging from 98 °C to 55 °C. Temperature profiles are provided for time intervals of 0 seconds, 1,800 seconds, 3,600 seconds, 5,400 seconds, and 7,200 seconds. Figure 18 presents the temperature profile within the thermal energy storage system (TES) tank. Subfigures A to E illustrate the 2D temperature fields, while subfigures (a) to (e) display the corresponding line plots. In these figures, blue indicates lower (colder) temperatures, and red signifies higher (hotter) temperatures. At time zero, the TES tank is at its initial uniform temperature of 98 °C.

By 1800 seconds, a thermocline layer characterized by a steep temperature gradient emerges around a height of 0.05 m. This sharp temperature transition, clearly visible in

Figure *12* (A–E), marks the thermocline, where the temperature shifts more rapidly than in other regions of the tank. As time advances, the thermocline zone moves upward: to approximately 0.15 m at 3600 seconds, 0.2 m at 5400 seconds, and 0.25 m at 7200 seconds. A steeper temperature curve indicates a thinner thermocline, which is preferable, as it reduces heat transfer from the hot fluid to the cold one. Over time, the thermocline layer becomes more diffuse due to prolonged thermal interaction between the hot and cold regions. Below the thermocline, the fluid temperature aligns with the cold inlet temperature, while above it, the fluid remains at a higher, heated state.

Figure 12

(A-E) 2D representation of the temperature profile inside the TES tank at 0, 1800, 3600, 5400, and 7200 seconds, respectively, for solid rocks. (a-e) Line diagrams of temperature versus tank height inside the TES tank at 0, 1800, 3600, 5400, and 7200 seconds, respectively.

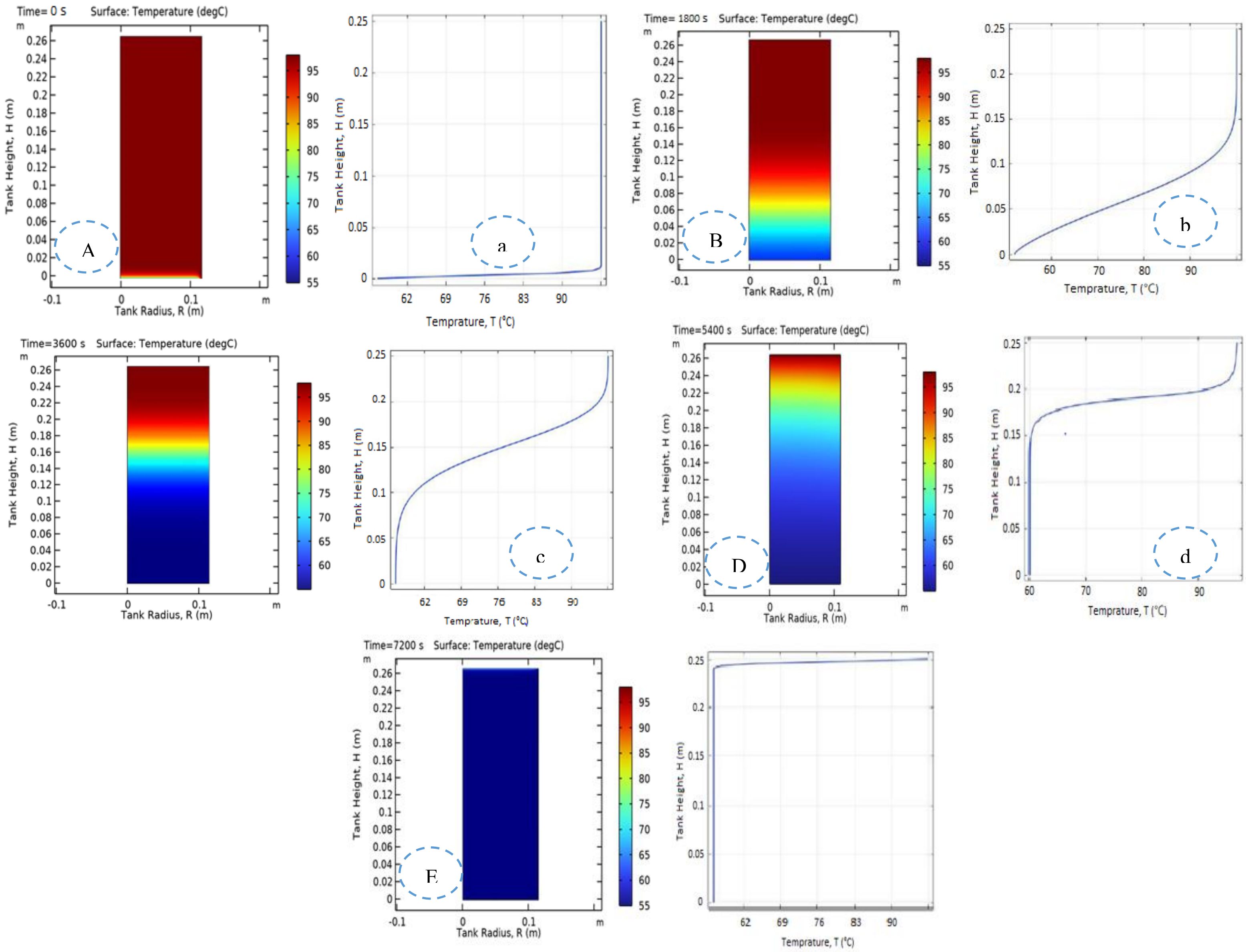

3.5 Enthalpy Vs Time during Charging and Discharging Process

Figure 13**,** titled "Enthalpy vs. Time during Charging (2D Axisymmetric TES)," illustrates the temporal variation of enthalpy (J/m^3) in a thermal energy storage (TES) system during the charging process. Over 0 to 7200 seconds, the enthalpy increases steadily from approximately 2.25 J/m^3 to around 2.55 J/m^3. This continuous rise signifies the absorption and storage of thermal energy within the system. The upward trend underscores the effective charging behavior of the thermal energy storage (TES) system, emphasizing the crucial role of enthalpy monitoring in optimizing energy storage efficiency. A comprehensive understanding of this behavior is vital for enhancing the performance and reliability of thermal energy systems across a wide range of applications.

Figure 13

Enthalpy vs Time during charging and Discharging (2D Axisymmetric TES).

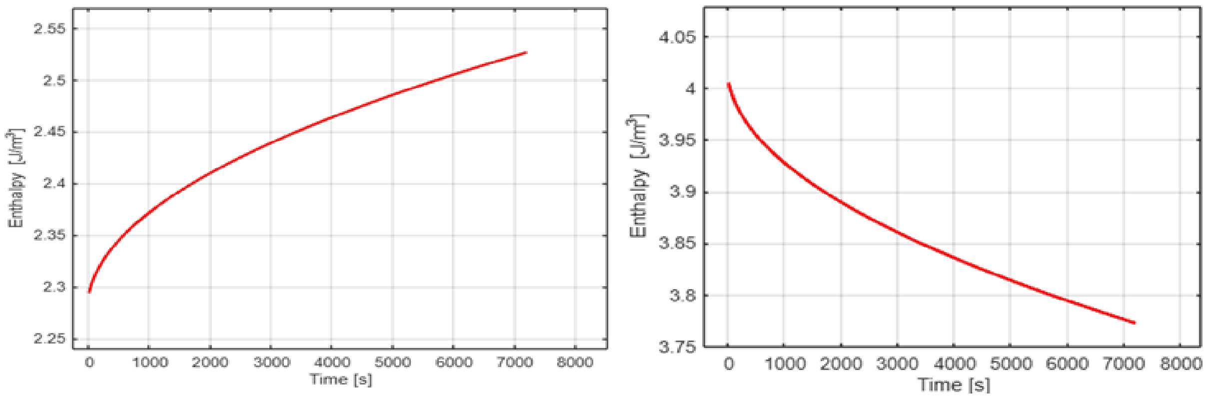

The above Figure 13 titled "Enthalpy vs. Time during Discharging (2D Axisymmetric TES)," illustrates the variation in enthalpy (J/m³) over time as a thermal energy storage (TES) system undergoes discharging. Over a period of 7,200 seconds, the enthalpy gradually decreases from approximately 4.0 J/m³ to around 3.75 J/m³, indicating the steady release of stored thermal energy. This downward trend highlights the effective discharge behavior of the TES, underscoring the importance of enthalpy tracking in managing energy output. A clear understanding of these dynamics is crucial for optimizing the performance and efficiency of TES systems in practical energy applications.

4. Conclusion and Recommendations

This study numerically investigated the performance of a single-tank thermocline thermal energy storage (TES) system for solar thermal applications in off-grid environments using water as the heat transfer fluid and low-cost solid filler materials. A two-dimensional Computational Fluid Dynamics (CFD) model based on the Finite Element Method (FEM) was developed to evaluate the system operating between 55°C and 98°C. During charging, a distinct thermocline with a thickness of approximately 0.263 m formed after 7200 s, producing strong thermal stratification and a charging efficiency of about 95%. Laminar flow was maintained throughout charging and discharging, with Reynolds numbers of approximately 1078 and 769, maximum velocities of 0.02 m/s and 0.002 m/s, respectively, and a stable pressure drop of about 2.49 kPa, confirming efficient heat storage, minimal thermal mixing, and stable flow behavior.

A structured quadrilateral mesh with a maximum element size of 0.1 m ensured mesh-independent and accurate simulations. During discharging, the thermocline moved upward while maintaining a sharp temperature gradient, demonstrating effective heat retention and energy recovery. Enthalpy analysis confirmed steady energy storage and release, highlighting the system's stable thermal performance. Overall, the results demonstrate that the water-based thermocline TES system provides efficient solar thermal storage with high thermal stratification, minimal mixing, and stable laminar flow, making it a promising solution for decentralized energy applications. Validation against published studies further confirmed the model's accuracy and reliability. Future work should investigate alternative heat transfer fluids and filler materials, extend the model to three-dimensional analyses, and include experimental validation and economic assessment to improve practical implementation.

Conflicts of Interest

The authors declare that they have no conflicts of interest with regard to the publication of this work.

Data Availability

Data used in this research are available from the corresponding author upon request.

References

Al, M. et. (2012). *Thermal Energy Storage System Comprising Encapsulated*. *1*(19), 1–11.

Alptekin, E., & Ezan, M. A. (2020). Performance investigations on a sensible heat thermal energy storage tank with a solar collector under variable climatic conditions. *Applied Thermal Engineering*, *164*, 114423. https://doi.org/10.1016/j.applthermaleng.2019.114423

Angelini, G., Lucchini, A., & Manzolini, G. (2014). Comparison of thermocline molten salt storage performances to commercial two-tank configuration. *Energy Procedia*, *49*(May), 694–704. https://doi.org/10.1016/j.egypro.2014.03.075

Atsbeha, A. K., Berhe, T. A., & Gebru, M. T. (2026). *Modelling and analysis of flat plate solar air collector with phase change materials for extended surface , drying application*.

Atsbeha, A. K., & Gebremariam, G. G. (2026). *Techno-Economic Feasibility Analysis of an Off-Grid Solar-Wind-Battery Hybrid Renewable Energy System for the Kara Adishuho Community , Northern Ethiopia*.

Atsbeha, A. K., Gebremariam, G. G., & Gebreslassie, T. H. (2024). Analysis of sunshine hours data and estimation of global solar radiation for Mychew Tabia Smret station , Northern. *Sustainable Energy Research*. https://doi.org/10.1186/s40807-024-00130-2

Atsbeha, A. K., Gebremariam, G. G., & Gebru, K. G. (2025). Assessment of solar resource potential and estimation of direct and diffuse solar irradiation from sunshine hours data for Eastern Zone of Tigray , Northern Ethiopia. *Sustainable Energy Research*. https://doi.org/10.1186/s40807-025-00162-2

Bayón, R., Rivas, E., & Rojas, E. (2014). Study of thermocline tank performance in dynamic processes and stand-by periods with an analytical function. *Energy Procedia*, *49*, 725–734. https://doi.org/10.1016/j.egypro.2014.03.078

Bayón, R., & Rojas, E. (2014). Analytical function describing the behaviour of a thermocline storage tank: A requirement for annual simulations of solar thermal power plants. *International Journal of Heat and Mass Transfer*, *68*, 641–648. https://doi.org/10.1016/j.ijheatmasstransfer.2013.09.070

Bonanos, A. M., & Votyakov, E. V. (2021). Analysis of thermocline

Disclosure Statement

No potential conflict of interest was reported by the author(s).

Additional Information

Funding

The authors received no financial support for the research, authorship, and/or publication of this article.

thermal energy storage systems with generic initial condition algebraic model. *Solar Energy*, *213*(December 2020), 154–162. https://doi.org/10.1016/j.solener.2020.11.011

Boubou, B., Kalawole Muritala, I., Makinta, B., Tizane, D., Guy Christian, T., Jacques, N., Téré, D., Antoine, B., & Rabani, A. (2021). Review on Thermocline Storage Effectiveness for Concentrating Solar Power Plant. *Energy and Power Engineering*, *13*(10), 343–364. https://doi.org/10.4236/epe.2021.1310024

Bouhlel, H. A., Gaha, R., Daaboul, J., & Chaker, A. (2023). Promoting Supply Chain Sustainability Through Industrial Packaging Eco-Designing. *Proceedings of the Design Society*, *3*(JULY), 2985–2993. https://doi.org/10.1017/pds.2023.299

Cascetta, M., Petrollese, M., Oyekale, J., & Cau, G. (2021). Thermocline vs. two-tank direct thermal storage system for concentrating solar power plants: A comparative techno-economic assessment. *International Journal of Energy Research*, *45*(12), 17721–17737. https://doi.org/10.1002/er.7005

Chang, Z., Li, X., Falcoz, Q., Wang, Z., Neveu, P., & Fasquelle, T. (2020). Approximate analytical characterization and multi-parametric optimization design of single-tank thermocline heat storage system. *Applied Thermal Engineering*, *181*(August), 116010. https://doi.org/10.1016/j.applthermaleng.2020.116010

Dincer, I. (2002). On thermal energy storage systems and applications in buildings. *Energy and Buildings*, *34*(4), 377–388. https://doi.org/10.1016/S0378-7788(01)00126-8

Dincer, I., & Rosen, M. A. (2011). Sustainability aspects of hydrogen and fuel cell systems. *Energy for Sustainable Development*, *15*(2), 137–146. https://doi.org/10.1016/j.esd.2011.03.006

Elfeky, K. E., Mohammed, A. G., & Wang, Q. wang. (2022). Performance analysis of an air rock thermocline TES tank for concentrated solar power plants using the coupled DEM–CFD approach. *Clean Technologies and Environmental Policy*, *24*(1), 3–19. https://doi.org/10.1007/s10098-021-02030-1

Fernández, F. J., Díaz, J., Folgueras, M. B., & Suárez, I. M. (2021). Stratification analysis and behaviour of a real industrial thermocline thermal energy storage tank for cogeneration purposes. *Processes*, *9*(1), 1–20. https://doi.org/10.3390/pr9010120

Flueckiger, S. M., & Garimella, S. V. (2012). Second-law analysis of molten-salt thermal energy storage in thermoclines. *Solar Energy*, *86*(5), 1621–1631. https://doi.org/10.1016/j.solener.2012.02.028

Flueckiger, S., Yang, Z., & Garimella, S. V. (2011). An integrated thermal and mechanical investigation of molten-salt thermocline energy storage. *Applied Energy*, *88*(6), 2098–2105. https://doi.org/10.1016/j.apenergy.2010.12.031

Guo, H., Elsihy, E. S., Liao, Z., & Du, X. (2021). Multi-Layer Encapsulated Phase Change Material Packed-Bed. *Energies*.

He, Z., Qian, Y., Xu, C., Yang, L., & Du, X. (2019). ScienceDirect ScienceDirect ScienceDirect Static and dynamic thermocline evolution in the water thermocline Static and dynamic thermocline evolution in the water thermocline storage tank storage tank Assessing the Yang heat. *Energy Procedia*, *158*(2018), 4471–4476. https://doi.org/10.1016/j.egypro.2019.01.766

He, Z., Wang, X., Du, X., Amjad, M., Yang, L., & Xu, C. (2019). Experiments on comparative performance of water thermocline storage tank with and without encapsulated paraffin wax packed bed. *Applied Thermal Engineering*, *147*, 188–197. https://doi.org/10.1016/j.applthermaleng.2018.10.051

Hoffmann, J., Fasquelle, T., Goetz, V., & Py, X. (2016). *A thermocline thermal energy storage system with filler materials for concentrated solar power plants : Experimental data and numerical model sensitivity to different experimental tank scales*. *100*, 753–761. https://doi.org/10.1016/j.applthermaleng.2016.01.110

Hu, C., Sun, M., Xie, Z., Yang, L., Song, Y., Tang, D., & Zhao, J. (2020). Numerical simulation on the forced convection heat transfer of porous medium for turbine engine heat exchanger applications. *Applied Thermal Engineering*, *180*(July), 115845. https://doi.org/10.1016/j.applthermaleng.2020.115845

Inlet, T. (2023). Thermocline Layer for Thermal Energy Storage. *ARANER Group*, 1–9.

Ismail, K. A. R., & Stuginsky, R. (1999). Parametric study on possible fixed bed models for pcm and sensible heat storage. *Applied Thermal Engineering*, *19*(7), 757–788. https://doi.org/10.1016/S1359-4311(98)00081-7

Jadhav, I. B., Bose, M., & Bandyopadhyay, S. (2020). Optimization of solar thermal systems with a thermocline storage tank. *Clean Technologies and Environmental Policy*, *22*(5), 1069–1084. https://doi.org/10.1007/s10098-020-01849-4

Junli, C., Yanping, Z., Chongzhe, Z., & Yulong, X. (2023). *Thermal performance analysis of a thermocline storage tank with integrated annular distributors*. *July*, 1–13. https://doi.org/10.3389/fenrg.2023.1190760

Kahsay, A., Goytom, D., Kidanu, A., Gebremicheal, K., & Tekleab, T. (2025). *Case Studies in Thermal Engineering Effect of multi-leg twisted tape inserts on heat transfer and pressure drop characteristics of a laminar pipe flow : A comparative analysis*. *74*(August).

Li, M. J., Qiu, Y., & Li, M. J. (2018). Cyclic thermal performance analysis of a traditional Single-Layered and of a novel Multi-Layered Packed-Bed molten salt Thermocline Tank. *Renewable Energy*, *118*, 565–578. https://doi.org/10.1016/j.renene.2017.11.038

Lou, W., Fan, Y., & Luo, L. (2020). Single-tank thermal energy storage systems for concentrated solar power: Flow distribution optimization for thermocline evolution management. *Journal of Energy Storage*, *32*(August), 101749. https://doi.org/10.1016/j.est.2020.101749

Lou, W., Luo, L., Hua, Y., Fan, Y., & Du, Z. (2021). A review on the performance indicators and influencing factors for the thermocline thermal energy storage systems. *Energies*, *14*(24), 1–19. https://doi.org/10.3390/en14248384

Mira-Hernández, C., Flueckiger, S. M., & Garimella, S. V. (2015). Comparative analysis of single- and dual-media thermocline tanks for thermal energy storage in concentrating solar power plants. *Journal of Solar Energy Engineering, Transactions of the ASME*, *137*(3). https://doi.org/10.1115/1.4029453

Qin, F. G. F., Yang, X., Ding, Z., Zuo, Y., Shao, Y., Jiang, R., & Yang, X. (2012). Thermocline stability criterions in single-tanks of molten salt thermal energy storage. *Applied Energy*, *97*, 816–821. https://doi.org/10.1016/j.apenergy.2012.02.048

Review, C. (2024). *New Advances in Materials , Applications , and Design*.

Şentürk Lüle, S., & Asaditaheri, A. (2022). Computational Fluid Dynamics Analysis of a Thermocline Thermal Storage Unit for Solar Thermal Applications. *Arabian Journal for Science and Engineering*, *47*(7), 9005–9018. https://doi.org/10.1007/s13369-021-06485-8

Types, A. A. (2024). ▯ *Menu Article*.

Yang, X., & Cai, Z. (2019). An analysis of a packed bed thermal energy storage system using sensible heat and phase change materials. *International Journal of Heat and Mass Transfer*, *144*, 118651. https://doi.org/10.1016/j.ijheatmasstransfer.2019.118651

Yang, Z., & Garimella, S. V. (2010). Thermal analysis of solar thermal energy storage in a molten-salt thermocline. *Solar Energy*, *84*(6), 974–985. https://doi.org/10.1016/j.solener.2010.03.007

Zhang, J., Terrones, M., Park, C. R., Mukherjee, R., Monthioux, M., Koratkar, N., Kim, Y. S., Hurt, R., Frackowiak, E., Enoki, T., Chen, Y., Chen, Y., & Bianco, A. (2016). Carbon science in 2016: Status, challenges and perspectives. *Carbon*, *98*, 708–732. https://doi.org/10.1016/j.carbon.2015.11.060

Zhu, C., Zhang, J., Wang, Y., Deng, Z., Shi, P., Wu, J., & Wu, Z. (2022). *applied sciences Study on Thermal Performance of Single-Tank Thermal Energy Storage System with Thermocline in Solar Thermal Utilization*.